Manuscript prepared for Clim. Past
with version 2015/04/24 7.83 Copernicus papers of the LaTeX class copernicus.cls.
Date: 24 June 2015

1200 years of warm-season temperature variability in central Fennoscandia inferred from tree-ring density

P. Zhang[1], H. W. Linderholm[1], B. E. Gunnarson[2], J. Björklund[3], and D. Chen[1]

[1]Regional Climate Group, Department of Earth Sciences, University of Gothenburg, Gothenburg, Sweden
[2]Bert Bolin Centre for Climate Research, Department of Physical Geography and Quaternary Geology, Stockholm University, Stockholm, Sweden
[3]Swiss Federal Research Institute WSL, Birmensdorf, Switzerland

Correspondence to: P. Zhang (peng.zhang@gvc.gu.se)

Abstract.

New collected Scots pine (*Pinus sylvestris* L.) tree-ring samples were used to replace the historical samples used in the previous central Scandinavia warm-season (April–September) temperature reconstruction, and to extend the reconstruction back to 850 CE. Since the new samples are collected from different elevations, and the samples from the different elevations do not cover the same period, the mean value of the samples was adjusted. The new reconstruction was produced based on "regional curve adjusted individual signal-free approach" (RSFi) which preserve mid- and long-term signal, and has better potential to remove unwanted noise (e.g. related to stand dynamics) on tree level. The new reconstruction, called C-Scan, suggests lower temperature during Medieval Climate Anomaly (MCA) and higher temperature during Little Ice Age (LIA) than the previous reconstruction. The two reconstructions show coherent variability at multidecadal to century timescales during the period 1300–2000 CE. Before 1300 CE, the two reconstructions show discrepancy especially for 1200–1250 CE. Comparing two independent summer temperature reconstructions from the northern Fennoscandia, C-Scan shows regional differences in temperature evolution at multidecadal to century timescales during MCA. The new reconstruction agrees with the general profile of northern hemisphere temperature evolution during the last 12 centuries, indicating the warm peak of MCA ca. 1009–1108 CE and the coldest period of LIA ca. 1550–1900 CE in central Fennoscandia. Moreover, in central Fennoscandia, during the past 1200 years, the coldest period was found in the late 17th–19th century with the coldest decades being centered on 1600 CE, and the warmest 100 years occurring in the most recent century.

1 Introduction

Fennoscandia has a strong tradition in dendrochronology, and its large tracts of boreal forest make the region well suited for the development of tree-ring chronologies that extend back over the last millennium (Linderholm et al., 2010). In addition to the well-known multi-millennial tree-ring width

chronologies from Torneträsk (Grudd et al., 2002), Finnish Lapland (Helama et al., 2002) and Jämtland (Gunnarson et al., 2003), several millennium long temperature-sensitive tree-ring datasets were collected within the European Union funded Millennium project (McCarroll et al., 2013). However, these were all, except for the Jämtland and Mora (822 year Blue intensity, Graham et al., 2011) records, located in northernmost Fennoscandia. It has been shown that in order to better represent Fennoscandian warm-season temperature variability, data from more southern locations are needed (Linderholm et al., 2014a). More recently, Helama et al. (2014) reconstructed May–September temperature variability in southern Finland (around 61° N) for the last millennium using maximum latewood density (MXD) data. In Sweden, the southernmost site to provide a robust temperature signal from tree-ring MXD data is the central Scandinavian Mountains, in the province of Jämtland, where Gunnarson et al. (2011, henceforth G11, referring to the temperature reconstruction) reconstructed 900 years of warm-season temperatures. Because of the relatively southerly location, Jämtland is considered a key location for paleotemperature studies in Scandinavia. Not only can it function as a link between chronologies in northern Fennoscandia and those in continental Europe (Gunnarson et al., 2011), but also the closeness to the North Atlantic makes it a suitable place to investigate long-term associations between marine and terrestrial climate variability (e.g., Cunningham et al., 2013).

At northern high latitudes, MXD is the most powerful warm-season temperature tree-ring proxy (Briffa et al., 2002a, b). The longest Scots pine MXD records have been sampled in northernmost Fennoscandia (see McCarroll et al., 2013; Melvin et al., 2013; Esper et al., 2012, 2014; Matskovsky and Helama , 2014). These chronologies are exclusively based on material with known temperature-sensitive provenience, from living trees, snags and, in the case of N-Scan, subfossil wood (tree remains which have been buried in lake sediments for hundreds or thousands of years) (Esper et al., 2012). G11, however, also included data collected from historical buildings in the Jämtland region in the late 1980s as a part of an archaeological survey by Kvartärbiologiska Laboratoriet in Lund, Sweden. Subsequently MXD was derived from some of these samples, which were later included in a dense MXD network covering cool moist regions in the northern hemisphere (Schweingruber et al., 1990). Due to the limited number of dead wood samples at that time from the studied area in the Scandinavian Mountains, the historical samples (covering the period between 1107 CE and 1827 CE, with a gap between 1292–1315 CE), made up a major part of G11. Since the geographical origins of the historical samples are somewhat unclear, where they likely originate from lowland locations about 300 meters below the present tree-line, it is not an optimal dataset to incorporate in a temperature reconstruction.

The Medieval Climate Anomaly (MCA, ca. 10th–13th CE, Grove and Switsur, 1994) is a period when the climate conditions in some regions are analogue to current warming, but without strong influences from human activities (Mann et al., 2009). This is a key period to evaluate if current warming can be reached without anthropogenic influences (Crowley and Lowery , 2000; Broecker ,

2001). However, there are few high-quality, annually resolved temperature reconstructions covering the MCA in the world (Mann et al., 2009; PAGES 2k Consortium , 2013). In the central Scandinavian Mountains, tree-ring data has shown excellent potential for reconstructing warm-season temperatures several centuries to millennia back in time (Linderholm and Gunnarson , 2005; Gunnarson et al., 2011). However, so far, the only MXD based temperature reconstruction from this region, G11, did not cover the whole MCA due to a lack of samples during this period.

Considering that 1) Jämtland is identified as a key dendroclimatological location in the Fennoscandian region, and 2) the fact that it does not cover the MCA in combination with 3) the questionable historical material of G11, the aim of this study is to extend the G11 temperature reconstruction and remove uncertainties of sampling provenances in the same. This will enable us to improve the understanding of the warm-season temperature evolution during the entire past 1200 years in this region, as well as make a more reliable comparison between the MCA and present conditions.

2 Data and method

2.1 Study area

The province of Jämtland is located in the westernmost part of central Sweden. The region belongs to the northern boreal zone, and the study area is situated just east of the Scandinavian Mountains main divide. The main topography ranges from 800 to 1000 $\mathrm{m\,a.s.l.}$, and scattered alpine massifs to the south reach approximately 1700 $\mathrm{m\,a.s.l.}$. There is a distinct climate gradient in the area (Linderholm et al., 2003). East of the Scandinavian Mountains, climate can be described as semi-continental. However, the proximity to the Norwegian Sea, lack of high mountains in the west, and the eastwest oriented valleys allow moist air to be advected from the ocean, providing an oceanic influence to the area (Johannessen , 1970; Johansson and Chen , 2003; Bojariu and Giorgi , 2005). Consequently, the study area is located in a border zone between oceanic and continental climates (Wallén , 1970). On short timescales, summer climate of this particular region is influenced by the atmospheric circulation, mainly the North Atlantic Oscillation (NAO) (Chen and Hellström, 1999), while it is affected by North Atlantic sea-surface temperature (SST) on longer timescales (Rodwell et al., 1999; Rodwell and Folland , 2002).

Glacial deposits dominate the area, mainly till but also glacifluvial deposits, peatlands and small areas of lacustrine sediments (Lundqvist, 1969). The forested parts in the central Scandinavian Mountains are dominated by Scots pine, Norway spruce (*Picea abies* (L.) H. Karst.) and mountain birch (*Betula pubescens*, Ehrh.). Although large-scale forestry have been carried out in most parts of the county, the human impact on trees growing close to the tree line is limited, which is valuable in tree-ring based climate reconstructions (Gunnarson et al., 2012). Due to the short and cool summers, snags can be preserved for more than 1000 years (Linderholm et al., 2014b). More-

over, large amounts of subfossil wood from hundreds to thousands of years ago can be found in small mountain lakes (see Gunnarson, 2008).

2.2 Tree-ring data and data statistics

The tree-ring data used in this study was sampled at eight sites (Table 1). As shown in Fig. 1, they are all in close proximity to each other, but differ in elevation and local environment. From the small peak Furuberget, 142 samples were collected close to the top at ca. 650 $\mathrm{m\,a.s.l.}$ in an open pine forest with limited competitions between trees. Pine trees grow on a relatively flat area covered by a thick vegetation layer with woody dwarf shrubs and mosses. The area is characterized by thin till and glacifluvial soils. 35 of these samples were included in G11 (Table 1). In addition, pine samples were collected at different elevations on Mount Håckervalen from the present tree line (at around 650 $\mathrm{m\,a.s.l.}$) up to 800 $\mathrm{m\,a.s.l.}$, described in detail in Linderholm et al. (2014b). Samples preserved in lakes (subfossil wood) were included from the lakes Lill-Rörtjärnen, Östra Helgtjärnen and Jens-Perstjärnen, and have previously been described in Gunnarson (2008). The historical tree-ring data, collected from historical buildings in the province was downloaded from the International Tree-Ring Data Bank (ITRDB).

The new MXD samples (Table 1) were measured using an ITRAX wood scanner from Cox Analytic System (http://www.coxsys.se). All the tree-ring samples were prepared according to Schweingruber et al. (1978). Thin laths (1.20 mm thick) were cut from each sample using a twin-bladed circular saw and subsequently resins and other compounds were extracted with pure alcohol in a Soxhlet apparatus. After being extracted for at least 24 hours, the laths were acclimatized in a room with controlled temperature and humidity to 12 $\%$ water content, and were then mounted in a sample holder. The samples were then exposed to a narrow, high energy, X-ray beam. The chrome tube in the ITRAX was tuned to 30 kV and 50 mA, with 75 ms steptime. The opening time of the sensor slit was set to 20 m at each step. From the detected X-ray radiation a 16-bit, greyscale, digital image with a resolution of 1270 dpi was captured. The grey levels were calibrated to values of wood density using a cellulose acetate calibration wedge provided by Walesch Electronics. The tree-ring MXD data were analysed with the image processing software WinDENDRO.

In Zhang et al. (2015), it was found that the MXD data used in this study, originating from various altitudes (Table. 1), likely differ in their mean values due to the environmental temperature lapse rates. In short, the MXD values at higher elevation were found to be systematically lower than those from lower elevation. Moreover, this influence on the MXD values was found to be larger than the temperature differences between warm MCA and the cold Little Ice Age (LIA, 14th-19th century according to Grove (2001)). Consider for example that older deadwood samples are found only at progressively higher elevations, even above present day tree line, as in Linderholm et al. (2014b), and that these samples are combined with lower elevation living trees and younger deadwood. If not accounted for, this may introduce serious biases to an averaged chronology, both in terms of

the annual to decadal variability, but perhaps even more so in the longer-term trends (Zhang et al., 2015). Therefore, we adjusted the mean MXD values from the different elevations to have the same mean during a period of overlap following the recommendations of Zhang et al. (2015). The mean MXD value of the Furuberget-north samples, covering 1300–1550 CE, was used as a reference for the adjustment of samples from other groups. The choice of Furuberget-north as a reference site was based on the criteria of a high sample replication and a wide temporal coverage.

2.3 Standardisation and chronology building

If tree-ring data is going to be used to attain reliable climate information, it is pertinent to remove as much non-climatic information as possible before building a chronology from the individual tree-ring series (Fritts, 1976). The non-climatological growth expression is usually represented with a least square fitted negative exponential function, polynomial or spline (Fritts, 1976; Cook and Peters, 1981), and subtracted or divided from each raw tree-ring measurement to obtain indices used for chronology building, in a process termed standardisation. This approach is widely used, but it severely limits the preservation of low-frequency variability in long chronologies (based on several generations of trees), because the mean value of all the tree-ring series will be adjusted to the same level after standardization. This is referred to as the "segment length curse" (Cook et al., 1995; Briffa et al., 1996).

This limitation can be overcome by quantifying the non-climatological growth expression for an entire population as an average of the growth of all samples aligned by cambial age, which then can be represented by a single mathematical function. Subsequently this function is subtracted from or divided by each individual tree-ring measurement, an approach called Regional Curve Standardisation (RCS; Briffa et al., 1992). However, by using one single function for all tree-ring series, mid-frequency noise (not climate-related signal) is not efficiently removed in the attempt to preserve the low-frequency (>segment length) variability (Melvin, 2004), along with possible trend distortion as described in (Melvin and Briffa, 2008; Melvin and Briffa , 2014a, b). Melvin and Briffa (2014a, b) show that using multi-curve RCS can, however, efficiently remove these biases. Alternatively, the non-climatological expression in tree-ring data can be quantified with an individual signal-free (SF) approach to standardisation, described in Melvin and Briffa (2008), but this approach is more limited in the lower most frequencies (Björklund et al., 2013).

However, by using the SF individual fitting approach and at the same time letting the derived functions to have a similar mean as their respective cambial age segment of the regional curve (RC) before subtraction into indices, stand competition etc. can also be addressed without losing the long timescale component (Björklund et al., 2013). This method, a hybrid of the RCS and individual SF standardization is henceforth referred to as RSFi. We produced chronologies with the standardisation methods: classic RCS, SF RCS (single curve and multi-curve) and RSFi, where the RSFi chronology was used for the new reconstruction. The standardisations were performed with the software

RCSsigFree (Cook et al., 2014) and CRUST (Melvin and Briffa , 2014a, b). The expressed population signal (EPS) criterion was used to evaluate the robustness of the chronology. An EPS value represents the percentage of the variance in the hypothetical population signal in the region that is accounted for by the chronology, where EPS values greater than 0.85 are generally regarded as sufficient (Wigley et al., 1984). In this study, the EPS values were calculated in a 50-year temporal window with 25-year overlap.

2.4 Instrumental data

Monthly temperature data from the closest meteorological station, Duved ($400\,\mathrm{m\,a.s.l.}$, $63.38^\circ\,\mathrm{N}$, $12.93^\circ\,\mathrm{E}$), was used to assess the temperature signal reflected by the chronology. Since the data from this station only cover the period 1911–1979 CE, we extended the data back to 1890 CE and up to 2011 CE by using linear regression on monthly temperature data from an adjacent station: Östersund ($376\,\mathrm{m\,a.s.l.}$, $63.20^\circ\,\mathrm{N}$, $14.49^\circ\,\mathrm{E}$). A linear regression was done to relate mean temperature of each month from Östersund station to that from Duved station. Data from Östersund explain on average $91.5\,\%$ of the interannual variance in Duved monthly temperature (based on the overlapping period 1911–1979 CE). The temperature data from Östersund came from two sources: the Nordklim data base (1890–2001 CE) (Tuomenvirta et al., 2001), and Swedish Meteorological and Hydrological Institute (SMHI, 2001–2011 CE). The locations of Duved and Östersund stations are shown in Fig. 1.

2.5 Climate signal in the new chronology

We compared the new chronology with the instrumental monthly mean temperatures constructed for the Duved meteorological station during the period 1890–2011 CE. Fig. 3a shows that the new chronology has a significant positive correlation (at $p < 0.01$ level) with individual monthly mean temperatures in April–September, and the highest correlation was found with mean April–September temperature ($r = 0.77$). Therefore, we decided to reconstruct the April–September mean temperature (henceforth referred to as warm-season temperature). The reconstructed and observed warm-season temperatures for 1890–2011 CE show a good agreement on interanual to multidecadal timescales (Fig. 3c), and the new MXD reconstruction explains $59\,\%$ of the variance in the instrumental data (Fig. 3b).

2.6 Reconstruction statistics

In order to test the temporal stability of the MXD vs. the instrumental observations, we divided the instrumental period into two parts: 1890–1950 CE and 1951–2011 CE, with the first part for calibration and the second part for verification. Then, we switched the calibration and verification periods, and repeated the same exercise. The calibration and verification statistics are shown in Table 2. The reduction of error statistic (RE) has a possible range of $-\infty$ to 1, and an RE of 1 can be achieved only if the prediction residuals equal zero. Zero is commonly used as a threshold, and

the positive RE values in the both calibration periods suggests that our reconstruction has some skill (Table 2). Similar to RE, coefficient of efficiency (CE) is a measure to evaluate the model under the validation period. Values close to zero or negative suggests that the reconstruction is no better than the mean, whereas positive values indicate the strength and temporal stability of the reconstruction.

We evaluated the spatial representativeness of the new warm-season temperature reconstruction by correlating it with the CRU TS3.22 $0.5^\circ \times 0.5^\circ$ gridded warm-season temperature (Harris et al., 2014) for the period 1901–2011 CE. We also compared the field correlation of observed warm-season temperature. As expected, Fig. 4 shows that the new reconstruction (4a) captures a large part of the patterns from the observations (4b). The reconstruction represents the warm-season temperature variation with correlations above 0.71 across much of central Fennoscandia, which validates the good spatial representativeness of our reconstruction.

3 Result and discussion

3.1 Comparing MXD samples of different origin

We compared the two chronologies based on the "in situ" and historical samples respectively. Three standardisation methods were applied to build the chronologies. Fig. 5 shows a comparison of the z scored (based on 1700–1800 CE) historical-sample chronology (HSC, blue curves) and the "in situ"- chronology (ISC, black curves) produced by the signal-free RCS (5a), negative exponential function standardisation (5b), and RSFi standardisation (5c) methods. Clearly, the same features can be observed regardless of the standardisation methods: 1) on multidecadal scales, the HSC agrees quite well with ISC between 1300 CE and 1800 CE, but the HSC displays a smaller variance than the ISC; 2) between 1100 CE and 1300 CE, there is a notable disagreement between HSC and ISC. On interannual scale (based on 1st difference chronologies), the HSC explain 34 % of variance in the ISC during 1100–1300 CE, and explain 62 % of the variance during 1300–1800 CE. Moreover, it should be noted that the EPS values fall below 0.85 for both chronologies during the 1160–1220 CE period. We tested boosting the ISC with the historical samples during 1100–1300 CE, but the EPS of the boosted chronology during 1160–1210 CE was still below 0.85, and the EPS during 1225–1265 CE was even smaller than before boosting. Only the EPS during 1212–1222 CE changed from below 0.85 to above 0.85. Consequently, there was no significant improvement of the robustness of the ISC during 1100–1300 CE after including the historical samples.

3.2 The influence of standardisation method

Presently, RCS and signal-free RCS (single- and multi-RCS curves) are the most favoured standardisation methods when building chronologies intended to have their long-term variability preserved. We examined the performances of the three above mentioned RCS methods as well as the RSFi method. As shown in Fig. 6, the difference among the four differently standardised chronologies is

mainly reflected in the multidecadal variability. The chronologies produced by the two single-curve RCS methods are in very good agreement on multidecadal timescales. The chronology produced by the multi-curve signal-free RCS methods differs from the ones based on single-curve RCS method, where it suggests warmer conditions over the past 1200 year, especially during the periods 930–1000 CE, 1270–1520 CE and 1620–1900 CE. The RSFi chronology, in turn, differs from all the three RCS ones, and it suggests slightly warmer conditions than the single-curve RCS based ones, especially pronounced during the late half of LIA, and colder condition than the multi-curve signal-free RCS chronology, especially pronounced during 1270–1550 CE. It is impossible to firmly state which one of the chronologies is closer to actual temperatures, but we argue that there is a benefit in using individual signal-free curves (the RSFi method) rather than a common regional signal-free curve or multi regional signal-free curve, since this procedure has a better potential to remove unwanted noise (e.g. related to stand dynamics) on tree level. Consequently, we opted for the RSFi chronology for the reconstruction.

3.3 Central Fennoscandian warm-season temperature evolution

Fig. 7 shows the reconstructed warm-season temperature in central Scandinavia, henceforth C-Scan, during the past 1200 years. C-Scan displays a cooling trend between 850 CE and 1800 CE, followed by a sharp temperature increase after the mid-19th century. In order to look at the C-Scan temperature evolution in more detail, we picked out the coldest and warmest periods (10, 30 and 100 years of mean temperatures respectively) during the last 1200 years (Fig. 7). The late 17th century to early 19th century was the coldest long-term period during the past 1200 years, and that the coldest 100-year period appeared during the 19th century. Both the coldest 10- and 30-year periods appeared during the 17th century. The warmest 100 years coincides with the most recent 100 years, which is consistent with the anthropogenic warming period (Stocker et al., 2013). However, the warmest 10- and 30-year periods were found in the 13th century. Comparing the MCA with the current warming period showed that the warmest 100-year period during the MCA was 0.1 °C cooler than the 20th century. The warmest 10- and 30-year periods during the 20th century were 0.2 °C and 0.1 °C cooler respectively than those during the 13th century. Despite low sample depth, the warmest 10- and 30-year periods have EPS values above 0.85.

3.4 The influence on MXD of elevation differences

To highlight the application of mean-adjusted data in our reconstruction, we compared reconstructions based on mean-adjusted and unadjusted samples. As shown in Fig. 8, the reconstruction based on unadjusted samples (blue curve) yields a 0.4 °C lower average warm-season temperature during the period 850–1200 CE compared to the mean-adjusted reconstruction (black curve). Moreover, the long-term trend before the onset of 12th century clearly differs between the two, where the cooling trend in the mean-adjusted data is turned to a warming trend in the unadjusted. Consequently,

a reconstruction based on unadjusted data would indicate that warm-season temperature in 850–1200 CE, roughly corresponding to the MCA, would be about 0.3 °C cooler than the subsequent four centuries (1201–1600 CE). This is contradictory to indications from other paleoclimate data for Fennoscandia (e.g., Esper et al., 2012; McCarroll et al., 2013; Melvin et al., 2013; Helama et al., 2014; Matskovsky and Helama , 2014), as well as for the extra-tropical northern hemisphere (Christiansen and Ljungqvist , 2012).

A previous way to deal with samples of different origin (living trees, subfossil and historical wood) or different sites, has been to use separate RCS curves for each type of sample (Gunnarson et al., 2011; Esper et al., 2012), but the prerequisite is that samples of different origin coexist in time, or at least have a large overlap, so that any differences in long-term trend are to a large extent cancelled out when averaging. Given that we did have some overlap between our different data, we could have used the "separate RCS curves" method. However, although this method produces a similar reconstruction after the mid-13th century, it provides a mean temperature for 850–900 CE and 1150–1250 CE that is 0.2 °C lower than by our preferred method.

3.5 Comparing C-Scan with the previous central Scandinavia tree-ring MXD warm-season temperature reconstruction

C-Scan was compared with G11, and as shown in Fig. 9, the new reconstruction suggests lower temperature during MCA and higher temperature during LIA than the previous one. The two reconstructions show coherent variability at multidecadal to century timescales during the period 1300–2000 CE. Before 1300 CE, the two reconstructions are less in agreement, especially during 1200–1250 CE. This could be due to the low sample depth in C-Scan at that time (see Fig. 7), but even though the sample depth was quite good in G11 during this period, it still shows low inter-series correlation (see Fig. 4 in Gunnarson et al., 2011) which suggests a lack of a coherent signal among the historical samples used in G11. The sample depth of C-Scan indicates a mortality phase during 1100–1200 CE following a rather strong regeneration phase during 1200–1350 CE. The strong regeneration of pine may result from successful establishment with good seed production on ground where is dominated by vegetation complexes favorable for seedling growth (Zachrisson et al., 1995).

3.6 Comparing C-Scan with two northern Fennoscandian summer temperature reconstructions

When comparing C-Scan with the most recently updated MXD reconstruction from northern Fennoscandia (NFENNO, as shown in Fig. 10) (Matskovsky and Helama , 2014), the same feature is noted as in the comparison with G11: consistent variability at multidecadal and century timescales after 1300 CE, except for 19th century, but less agreement before 1300 CE. It is clear that the low sample depth causes the offset during the 13th century, and hence, work on increasing the sample depth of the period before 1300 CE is still needed in central Scandinavia. Another notable feature is

that NFENNO indicates higher summer temperatures in northern Fennoscandia than that in central Scandinavia during the 10th–11th centuries. When comparing C-Scan with the tree-ring multiproxy summer temperature reconstruction from northern Fennoscandia (McCarroll et al., 2013), the latter suggests a similar or slightly colder summer temperature in northern Fennoscandia than in central Scandinavia during 10th–11th centuries. It is difficult to say which reconstruction in northern Fennoscandia represents a true temporal evolution of summer temperature. However, the difference between central and northern Fennoscandia may actually reflect a true difference in temporal evolutions of summer temperature, which could be related to changes in the large-scale circulation affecting the region. Possibly changes in the spatial positions of the nodes of the NAO dipole over time (Ulbrich and Christoph , 1999; Zhang et al., 2008) could cause disruptions in the usually coherent summer temperature pattern over Fennoscandia. Both reconstructed and observed surface temperature evolutions show differences in their magnitudes in central and northern Scandinavia in some time intervals during the last millennium (Ljungqvist et al., 2012) and the 20th century (Diaz et al., 2011), which support the possibility of differences in regional temperature evolution. Since the instrumental record is too short, the mechanism behind this needs to be investigated, for example with assistance of climate models. C-Scan also shows larger variance than the two summer reconstructions from northern Fennoscandia during some periods, and this is likely due to C-Scan being based on samples collected from a confined area, whereas the two northern reconstructions are from multi-sites in much larger areas.

3.7 Comparing C-Scan with an extra-tropical northern hemisphere mean temperature reconstruction

C-Scan was also compared to the extra-tropical northern hemisphere (NH) multi-proxy annual mean temperature reconstruction from Christiansen and Ljungqvist (2012) in order to place it into a large spatial context. From Fig. 11, we see that both records show a general cooling trend during the last millennium which is consistent with long-term astronomical forcing (Mann et al., 1999). However, the cooling is stronger in the large-scale reconstruction. This is likely due to the NH reconstruction being partly based on low-resolution paleo archives which have larger variance at millennium timescales (Moberg et al., 2005). Another reason could be that some of the paleo archives can also represent annual mean temperature evolution whose trend could be different with C-Scan (Cohen et al., 2012). C-Scan suggests a warm MCA peak between 1000–1100 CE, while the NH reconstruction suggests a longer warm peak between 950–1150 CE. This could implicate that the warm maximum during MCA in central Scandinavia comes later than at some other places in the extra-tropical northern hemisphere, since the temperature evolutions in different regions have shown differences in their timing and magnitude during MCA (PAGES 2k Consortium , 2013). However, the seasonal differences in temperature evolution, as mentioned above, could also be the reason of the discrepancy of the warm maximum between the two reconstructions. Both reconstructions show that the

coldest multi-century periods occur during 1600–1900 CE. Moreover, the two reconstructions show less coherent variability during the period 950–1300 CE (corresponding to MCA). The temperature evolution difference during this period has been detected from many paleoclimate reconstructions from regional, continental to hemispheric scale (PAGES 2k Consortium , 2013; Masson-Delmotte et al., 2013). In order to make clear the temperature evolution during MCA, efforts should be made to increase the number of high-temporal resolution temperature reconstruction during this period. In another aspect, the reasons of the differences in regional temperature evolution should be also investigated from circulation perspectives.

4 Conclusions

An updated and extended version of the Jämtland MXD chronology was used to reconstruct the warm-season mean temperature (April–September) evolution in central Fennoscandia for the period 850–2011 CE. Due to the fact that the samples come from different elevations, the new reconstruction, called C-Scan, was based on mean-adjusted data subsequently standardised using the RSFi method. Our new reconstruction suggests a MCA warm-peak during ca. 1000 CE to 1100 CE, followed by a transition period before the onset of the Little Ice Age proper in the mid-16th century. During the last 1200 years, the late 17th century to early 19th century was the coldest period in central Fennoscandia, and the warmest 100 years occurred during the most recent century in central Fennoscandia, and the coldest decades occurred around 1600 CE. The new reconstruction suggests lower temperature during the late MCA (ca. 1100–1220 CE) and higher temperature during the LIA (1610–1850 CE) than the previous reconstruction (G11) from the region. Comparing C-Scan to two independent summer temperature reconstructions from northern Fennoscandia, regional differences in temperature evolution are notable before 1300 CE. The difference may reflect a true difference in temporal evolutions of summer temperature, which could be related to changes in the large-scale circulation affecting the region, or they could be caused by low sample replication.

Acknowledgements. We acknowledge the County Administrative Boards of Jämtland for giving permissions to conduct dendrochronological sampling, and Mauricio Fuentes, Petter Stridbeck, Riikka Salo, Emad Farahat and Eva Rocha for their help in the field. We also thank Laura McGlynn and Håkan Grudd for assistance in the MXD measurements and Andrea Seim for helping out with GIS and correcting the manuscript. This work was supported by Grants from the two Swedish research councils (Vetenskapsrådet and Formas, Grants to Hans Linderholm) and the Royal Swedish Academy of Sciences (Kungl. Vetenskapsakademien, grant to Peng Zhang). This research contributes to the strategic research areas Modelling the Regional and Global Earth system (MERGE), and Biodiversity and Ecosystem services in a Changing Climate (BECC) and to the PAGES2K initiative. This is contribution # 33 from the Sino-Swedish Centre for Tree-Ring Research (SISTRR).

References

Björklund, J. A., Gunnarson, B. E., Krusic, P. J., Grudd, H., Josefsson, T., Östlund, L., and Linderholm, H. W.: Advances towards improved low-frequency tree-ring reconstructions, using an updated Pinus sylvestris L. MXD network from the Scandinavian Mountains, Theor. Appl. Climatol., 113, 697–710, 2013.

Bojariu, R. and Giorgi, F.: The North Atlantic Oscillation signal in a regional climate simulation for the European region, Tellus A, 57(4), 641–653, 2005.

Briffa, K. R., Jones, P. D., Bartholin, T. S., Eckstein, D., Schweingruber, F. H., Karlen, W., Zetterberg, P., and Eronen, M.: Fennoscandian summers from AD 500: temperature changes on short and long timescales, Clim. Dynam., 7, 111–119, 1992.

Briffa, K. R., Jones, P. D., Schweingruber, F. H., Karlén, W., and Shiyatov, S. G.: Tree-Ring Variables as Proxy-Climate Indicators: Problems with Low-Frequency Signals, Springer, 9–41, 1996.

Briffa, K. R., Osborn, T. J., Schweingruber, F. H., Jones, P. D., Shiyatov, S. G., and Vaganov, E. A.: Tree-ring width and density data around the Northern Hemisphere: Part 1, local and regional climate signals, The Holocene, 12, 737–757, 2002a.

Briffa, K. R., Osborn, T. J., Schweingruber, F. H., Jones, P. D., Shiyatov, S. G., and Vaganov, E. A.: Tree-ring width and density data around the Northern Hemisphere: Part 2, spatio-temporal variability and associated climate patterns, The Holocene, 12, 759–789, 2002b.

Broecker, W. S.: Paleoclimate: was the medieval warm period global?. Science, 291(5508), 1497–1499, doi:10.1126/science.291.5508.1497, 2001.

Chen, D. and Hellström, C.: The influence of the North Atlantic Oscillation on the regional temperature variability in Sweden: spatial and temporal variations, Tellus A, 51, 505–516, 1999.

Christiansen, B. and Ljungqvist, F. C.: The extra-tropical Northern Hemisphere temperature in the last two millennia: reconstructions of low-frequency variability. Climate of the Past, 8(2), 765–786, 2012.

Cohen, J. L., Furtado, J. C., Barlow, M., Alexeev, V. A., and Cherry, J. E.: Asymmetric seasonal temperature trends, Geophysical Research Letters, 39(4), doi:10.1029/2011GL050582, 2012.

Cook, E. R. and Peters, K.: The Smoothing Spline: A New Approach to Standardizing Forest Interior Tree-Ring width Series for Dendroclimatic Studies, 1981.

Cook, E. R., Briffa, K. R., Meko, D. M., Graybill, D. A., and Funkhouser, G.: The "segment length curse" in long tree-ring chronology development for palaeoclimatic studies, The Holocene, 5, 229–237, 1995.

Cook, E. R., Krusic, P. J., and Melvin, T.: Program RCSsigFree: Version 45_v2b. Lamont-Doherty Earth Obs. Columbia University, 2014.

Crowley, T. J. and Lowery, T. S.: How warm was the medieval warm period? AMBIO: A Journal of the Human Environment, 29(1), 51–54, 2000.

Cunningham, L. K., Austin, W. E., Knudsen, K. L., Eiríksson, J., Scourse, J. D., Wanamaker, A. D., Butler, P. G., Cage, A. G., Richter, T., and Husum, K.: Reconstructions of surface ocean conditions from the northeast Atlantic and Nordic seas during the last millennium, The Holocene, 23, 921–935, 2013.

Diaz, H. F., Trigo, R., Hughes, M. K., Mann, M. E., Xoplaki, E., and Barriopedro, D.: Spatial and temporal characteristics of climate in medieval times revisited. Bulletin of the American Meteorological Society, 92(11), 1487–1500, 2011.

Esper, J., Frank, D. C., Timonen, M., Zorita, E., Wilson, R. J., Luterbacher, J., Holzkämper, S., Fischer, N., Wagner, S., and Nievergelt, D.: Orbital forcing of tree-ring data, Nature Climate Change, 2, 862–866, 2012.

Esper, J., Duethorn, E., Krusic, P. J., Timonen, M., and Buentgen, U.: Northern European summer temperature variations over the Common Era from integrated treering density records, Journal of Quaternary Science, 29(5), 487–494, 2014.

Fritts, H.: Tree Rings and Climate, ACADEMIC PRESS INC. (LONDON) LTD, London, UK, 1976.

Graham, R., Robertson, I., McCarroll, D., Loader, N., Grudd, H., and Gunnarson, B.: Blue Intensity in Pinus sylvestris: application, validation and climatic sensitivity of a new palaeoclimate proxy for tree ring research, in: AGU Fall Meeting Abstracts, vol. 1, p. 1896, 9–41, 2011.

Grove, J. M.: The Initiation of the "Little Ice Age" in Regions Round the North Atlantic, Springer, 53–82, 2001.

Grove, J. M. and Switsur, R.: Glacial geological evidence for the Medieval Warm Period, Climatic Change, 26, 143–169, 1994.

Grudd, H., Briffa, K. R., Karlén, W., Bartholin, T. S., Jones, P. D., and Kromer, B.: A 7400-year tree-ring chronology in northern Swedish Lapland: natural climatic variability expressed on annual to millennial timescales, The Holocene, 12, 657–665, 2002.

Gunnarson, B. E.: Temporal distribution pattern of subfossil pines in central Sweden: perspective on Holocene humidity fluctuations, The Holocene, 18, 569–577, 2008.

Gunnarson, B. E., Borgmark, A., and Wastegård, S.: Holocene humidity fluctuations in Sweden inferred from dendrochronology and peat stratigraphy, Boreas, 32, 347–360, 2003.

Gunnarson, B. E., Linderholm, H. W., and Moberg, A.: Improving a tree-ring reconstruction from west-central Scandinavia: 900 years of warm-season temperatures, Clim. Dynam., 36, 97–108, 2011.

Gunnarson, B. E., Josefsson, T., Linderholm, H. W., and Östlund, L.: Legacies of pre-industrial land use can bias modern tree-ring climate calibrations, Clim. Res., 53, 63–76, 2012.

Harris, I., Jones, P., Osborn, T., and Lister, D.: Updated high resolution grids of monthly climatic observations – the CRU TS3. 10 Dataset, Int. J. Climatol., 34, 623–642, 2014.

Helama, S., Lindholm, M., Timonen, M., Meriläinen, J., and Eronen, M.: The supra-long Scots pine tree-ring record for Finnish Lapland: Part 2, interannual to centennial variability in summer temperatures for 7500 years, The Holocene, 12, 681–687, 2002.

Helama, S., Vartiainen, M., Holopainen, J., Mäkelä, H. M., Kolström, T., and Meriläinen, J.: A palaeotemperature record for the Finnish Lakeland based on microdensitometric variations in tree rings, Geochronometria, 41, 265–277, 2014.

Johannessen, T. W.: The climate of Scandinavia, Climates of Northern and Western Europe, World survey of climatology, 5, 23–80, 1970.

Johansson, B. and Chen, D.: The influence of wind and topography on precipitation distribution in Sweden: Statistical analysis and modelling, International Journal of Climatology, 23(12), 1523–1535, 2003.

Linderholm, H. W., Solberg, B. Ø., and Lindholm, M.: Tree-ring records from central Fennoscandia: the relationship between tree growth and climate along a westeast transect, The Holocene, 13(6), 887–895, 2003.

Linderholm, H. W., and Gunnarson, B. E.: Summer temperature variability in central Scandinavia during the last 3600 years, Geografiska Annaler: Series A, Physical Geography, 87(1), 231–241, 2005.

Linderholm, H. W., Björklund, J. A., Seftigen, K., Gunnarson, B. E., Grudd, H., Jeong, J.-H., Drobyshev, I., and Liu, Y.: Dendroclimatology in Fennoscandia – from past accomplishments to future potential, Clim. Past, 6, 93–114, doi:10.5194/cp-6-93-2010, 2010.

Linderholm, H., Björklund, J., Seftigen, K., Gunnarson, B., and Fuentes, M.: Fennoscandia revisited: a spatially improved tree-ring reconstruction of summer temperatures for the last 900 years, Clim. Dynam., 1–15, doi:10.1007/s00382-014-2328-9, 2014a.

Linderholm, H. W., Zhang, P., Gunnarson, B. E., Björklund, J., Farahat, E., Fuentes, M., Rocha, E., Salo, R., Seftigen, K., and Stridbeck, P.: Growth dynamics of tree-line and lake-shore Scots pine (Pinus sylvestris L.) in the central Scandinavian Mountains during the Medieval Climate Anomaly and the early Little Ice Age, Paleoecology, 2, 20, doi:10.3389/fevo.2014.00020, 2014b.

Ljungqvist, F. C., Krusic, P. J., Brattström, G., and Sundqvist, H. S.: Northern Hemisphere temperature patterns in the last 12 centuries, Clim. Past, 8, 227–249, doi:10.5194/cp-8-227-2012, 2012.

Lundqvist, J.: Beskrivning till jordartskarta över Jämtlands län: 4 Karten. Kt, Sveriges Geologiska Undersökning, 1969.

Mann, M. E., Bradley, R. S., and Hughes, M. K.: Northern Hemisphere temperatures during the past millennium, Geophysical Research Letters, 4(6), 759–762, 1999.

Mann, M. E., Zhang, Z., Hughes, M. K., Bradley, R. S., Miller, S. K., Rutherford, S., and Ni, F.: Proxy-based reconstructions of hemispheric and global surface temperature variations over the past two millennia, Proceedings of the National Academy of Sciences, 105(36), 13252–13257, 2008.

Mann, M. E., Zhang, Z., Rutherford, S., Bradley, R. S., Hughes, M. K., Shindell, D., Ammann, C., Faluvegi, G., and Ni, F.: Global signatures and dynamical origins of the Little Ice Age and Medieval Climate Anomaly, Science, 326(5957), 1256–1260, 2009.

Masson-Delmotte, V., Schulz, M., Abe-Ouchi, A., Beer, J., Ganopolski, A., González Rouco, J. F., Jansen, E., Lambeck, K., Luterbacher, J., Naish, T., Osborn, T., Otto-Bliesner, B., Quinn, T., Ramesh, R., Rojas, M., Shao, X., and Timmermann, A.: Information from Paleoclimate Archives. In: Climate Change 2013: The Physical Science Basis. Contribution of Working Group I to the Fifth Assessment Report of the Intergovernmental Panel on Climate Change [Stocker, T. F., Qin, D., Plattner, G. -K., Tignor, M., Allen, S. K., Boschung, J., Nauels, A., Xia, Y., Bex, V., and Midgley, P. M. (eds.)]. Cambridge University Press, Cambridge, United Kingdom and New York, NY, USA, 383–464, doi:10.1017/CBO9781107415324.013,2013.

Matskovsky, V. V. and Helama, S.: Testing long-term summer temperature reconstruction based on maximum density chronologies obtained by reanalysis of tree-ring data sets from northernmost Sweden and Finland, Climate of the Past, 10(4), 1473–1487, 2014.

McCarroll, D., Loader, N. J., Jalkanen, R., Gagen, M. H., Grudd, H., Gunnarson, B. E., Kirchhefer, A. J., Friedrich, M., Linderholm, H. W., and Lindholm, M.: A 1200-year multiproxy record of tree growth and summer temperature at the northern pine forest limit of Europe, The Holocene, 0, 1–14, 2013.

Melvin, T. M.: Historical Growth Rates and Changing Climatic Sensitivity of Boreal Conifers, University of East Anglia, Norwich, UK, 2004.

Melvin, T. M. and Briffa, K. R.: A "signal-free" approach to dendroclimatic standardisation, Dendrochronologia, 26, 71–86, 2008.

Melvin, T. M., Grudd, H., and Briffa, K. R.: Potential bias in "updating" tree-ring chronologies using regional curve standardisation: re-processing 1500 years of Torneträsk density and ring-width data, The Holocene, 23, 364–373, 2013.

Melvin, T. M., Briffa, K. R.: CRUST: Software for the implementation of regional chronology standardisation: part 1. Signal-free RCS, Dendrochronologia, 32(1), 7–20, 2014a.

Melvin, T. M., Briffa, K. R.: CRUST: Software for the implementation of Regional Chronology Standardisation: Part 2. Further RCS options and recommendations, Dendrochronologia, 32(4), 343–356, 2014b.

Moberg, A., Sonechkin, D. M., Holmgren, K., Datsenko, N. M., and Karlén, W.: Highly variable Northern Hemisphere temperatures reconstructed from low- and high-resolution proxy data, Nature, 433(7026), 613–617, 2005.

PAGES 2k Consortium: Continental-scale temperature variability during the last two millennia, Nature Geoscience, 6, 339–346, doi:10.1038/ngeo1797, 2013.

Rodwell, M. and Folland, C.: Atlantic air–sea interaction and seasonal predictability, Q. J. Roy. Meteor. Soc., 128, 1413–1443, 2002.

Rodwell, M., Rowell, D., and Folland, C.: Oceanic forcing of the wintertime North Atlantic Oscillation and European climate, Nature, 398, 320–323, 1999.

Schweingruber, F., Fritts, H., Bräker, O., Drew, L., and Schär, E.: The X-Ray Technique as Applied to Dendroclimatology, 1978.

Schweingruber, F., Kairiukstis, L., and Shiyatov, S.: Sample Selection, Methods of Dendrochronology: Applications in the Environmental Sciences, 23–35, 1990.

Stocker, T., Qin, D., Plattner, G., Tignor, M., Allen, S., Boschung, J., Nauels, A., Xia, Y., Bex, V., and Midgley, P.: IPCC, 2013: summary for policymakers, in: Climate Change 2013: The Physical Science Basis, Contribution of Working Group I to the Fifth Assessment Report of the Intergovernmental Panel on Climate Change, Cambridge Univ. Press, Cambridge, UK, 3–29, 2013.

Tuomenvirta, H., Drebs, A., Førland, E., Tveito, O. E., Alexandersson, H., Laursen, E. V., and Jónsson, T.: Nordklim data set 1.0 description and illustrations, Tech. rep., DNMI Report, 2001.

Ulbrich, U. and Christoph, M.: A shift of the NAO and increasing storm track activity over Europe due to anthropogenic greenhouse gas forcing, Climate dynamics, 15(7), 551–559, 1999.

van Oldenborgh, G. J., Drijfhout, S., van Ulden, A., Haarsma, R., Sterl, A., Severijns, C., Hazeleger, W., and Dijkstra, H.: Western Europe is warming much faster than expected, Clim. Past, 5, 1–12, doi:10.5194/cp-5-1-2009, 2009.

Wallén, C. C. (ed.) Climates of Northern and Western Europe, Elsevier, Amsterdam, 1970.

Wigley, T. M., Briffa, K. R., and Jones, P. D.: On the average value of correlated time series, with applications in dendroclimatology and hydrometeorology, J. Clim. Appl. Meteorol., 23, 201–213, 1984.

Zachrisson, O., Nilsson, M-C., Steijlen, I., and Hörnberg, G.: Regeneration pulses and climate-vegetation interactions in nonpyrogenic boreal Scots pine stands, Journal of Ecology, 83, 469–83, 1995.

Zhang, P., Björklund, J., and Linderholm, H. W.: The influence of elevational differences in absolute maximum density values on regional climate reconstructions, Trees, 1–13, doi:10.1007/s00468-015-1205-4, 2015.

Zhang, X., Sorteberg, A., Zhang, J., Gerdes, R., and Comiso, J. C.: Recent radical shifts of atmospheric circulations and rapid changes in Arctic climate system, Geophysical Research Letters, 35(22), 2008.

Table 1. Tree-ring sampling sites and summary statistics of the MXD data.

Sampling sites	Elev	TS	NS	MTA	AMXD	MS	AC1
Furuberget-north	650	873–1112	3	156	0.74	0.118	0.556
		1189–2005	104	168	0.69	0.122	0.571
Furuberget-south (G11)	650	1497–2008	35	193	0.64	0.133	0.457
Håckervalen-south	750	783–1265	30	130	0.66	0.125	0.415
		1276–1520	24	113	0.60	0.134	0.449
Håckervalen-north	650	1778–2011	5	213	0.71	0.165	0.314
Lilla-Rörtjärnen*	560	952–1182	13	90	0.67	0.122	0.572
		1290–1668	9	147	0.63	0.122	0.655
		1750–1861	1	112	–	–	–
Öster Helgtjärnen*	646	929–1093	6	121	0.62	0.124	0.715
		1119–1333	3	104	0.72	0.122	0.625
		1336–1402	1	67	–	–	–
		1446–1568	2	110	0.76	0.106	0.676
Jens Perstjärnen*	700	1196–1382	2	153	0.62	0.133	0.753
Historical buildings	< 500	1107–1291	15	158	0.84	0.082	0.676
(Jämtland, Sweden)		1316–1827	118	161	0.79	0.089	0.576

Elev: source elevation (m a.s.l); TS: time span (CE); NS: number of samples; MTA: mean tree age (year); AMXD: average MXD ($\mathrm{g\,cm^{-3}}$); MS: mean sensitivity; AC1: first-order autocorrelation; * means that the sampling site is a lake. Some of the "mean tree ages" are less than 100 years, because the MXD measurement is only a part of a tree-ring width measurement which is much longer. The cutting of the samples is due to that some parts of the samples were too rotten for MXD to be measured. Tree-ring data from Furuberget-north, Håckervalen-south, Håckervalen-north, Lilla-Rörtjen, Öster Helgtjärnen and Jens Perstjärnen are newly added data. Tree-ring data from historical buildings are downloaded from International Tree-Ring Data Bank (ITRDB), which has been used in the previous tree-ring MXD based warm-season temperature reconstruction (the G11). In this paper, the historical building data was used in the analysis, but was not used for the new temperature reconstruction, while tree-ring data from other sites were used in the new reconstruction.

Table 2. Calibration and verification statistics of the warm-season temperature reconstruction.

MXD RSFi chronology			
Calibration period	1890–1950	1951–2011	1890–2011
Correlation, R	0.82[a]	0.67[a]	0.77[a]
Explained variance, R^2	0.67	0.46	0.59
No. of observations	61	61	122
Verification period	1951–2011	1890–1950	–
Explained variance, R^2	0.46	0.67	–
RE[b]	0.55	0.71	–
CE[b]	0.44	0.65	–

[a] the correlation is significant at $p < 0.01$ significance level; [b] RE means reduction of error; CE means coefficient of efficiency.

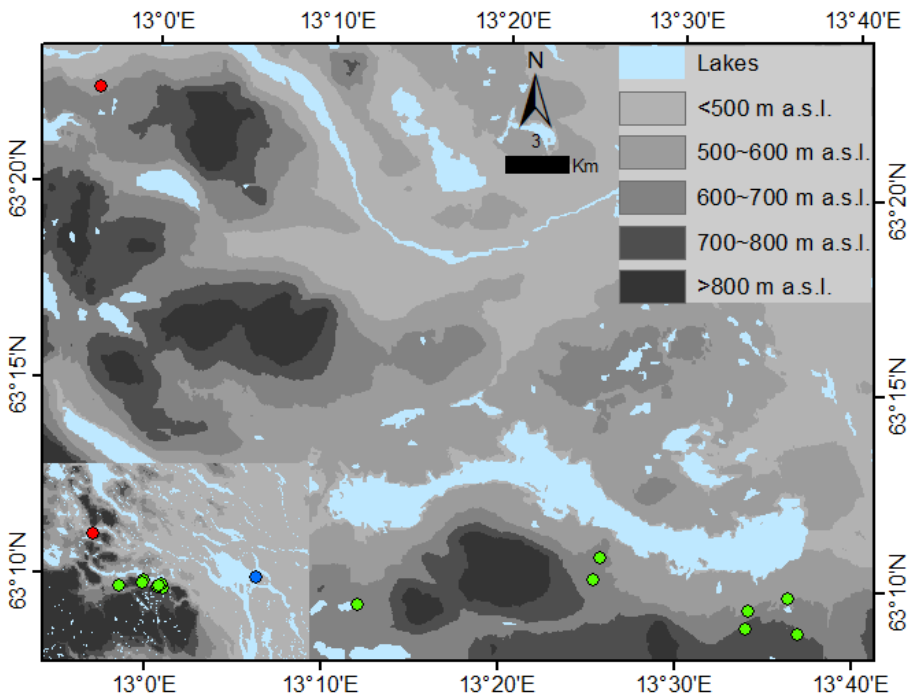

Figure 1. Map showing the locations of tree-ring sampling sites (green dots), except for historical samples, and Duved (red dot) and Östersund (blue dot) meterological station.

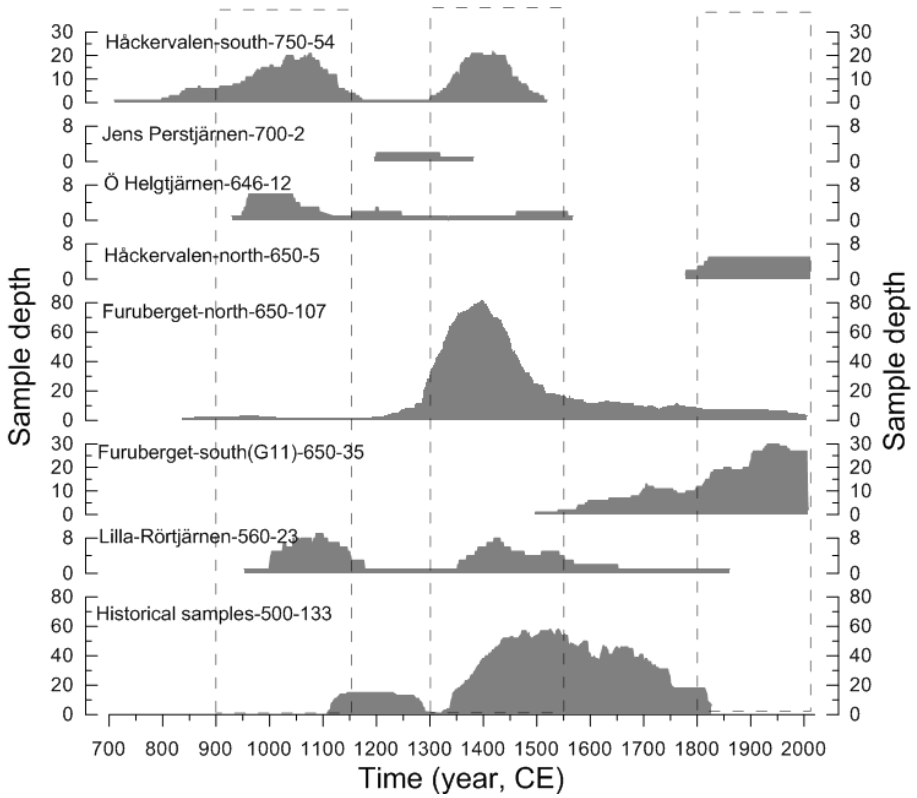

Figure 2. Sample replication and time span in each site/group. The site/group names, elevations and the number of samples were given on the upper left corner of each subplot. Dashed line frames mark three common periods with most of the samples.

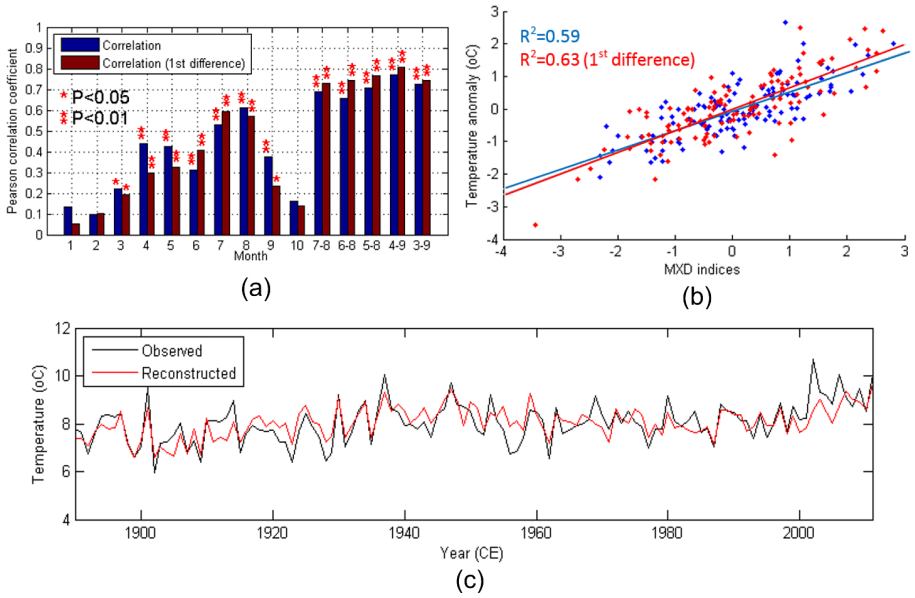

Figure 3. **(a)** Correlation between the mean-adjusted MXD data, standardised with RSFi method, and monthly mean temperature over the period 1890–2011 CE. Correlations are given from January to October of the growth year and July–August, June–August, May–August, April–September (warm season) and March–September average; **(b)** Linear relationship between MXD data and warm-season temperature (anomaly relative to 1961–1990 mean (blue) and 1st difference (red)); **(c)** comparison of reconstructed warm-season temperature (red) with observed Duved warm-season temperature (black) for the period 1890–2011 CE.

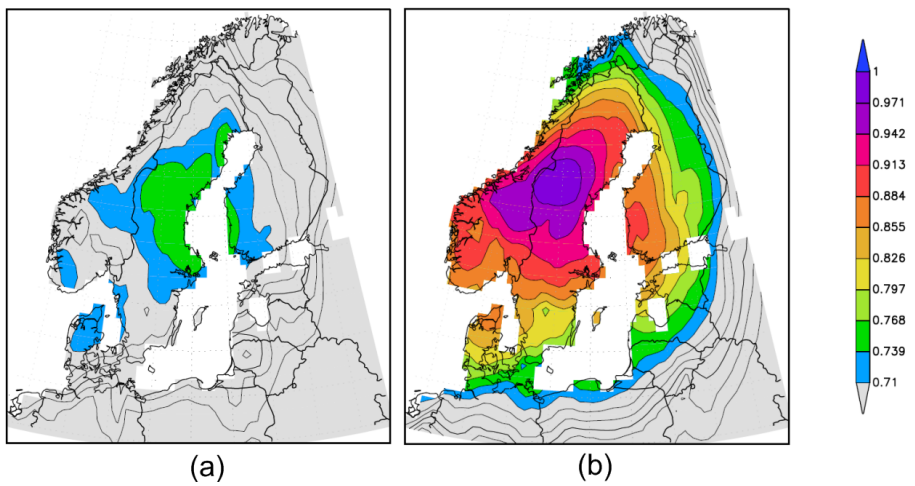

Figure 4. Field correlations of the reconstructed warm-season temperature from **(a)** the new chronology in this study and **(b)** observed Duved warm-season temperature with the gridded warm-season temperature from CRU TS3.22 $0.5^\circ \times 0.5^\circ$ dataset during the period 1901–2011 CE. Grey areas outside the $r = 0.71$ isoline represent the correlations at $p < 0.001$ significance level. The field correlation maps were plotted using the "KNMI climate explorer" (Royal Netherlands Meteorological Institute; http://climexp.knmi.nl; Van Oldenborgh et al., 2009).

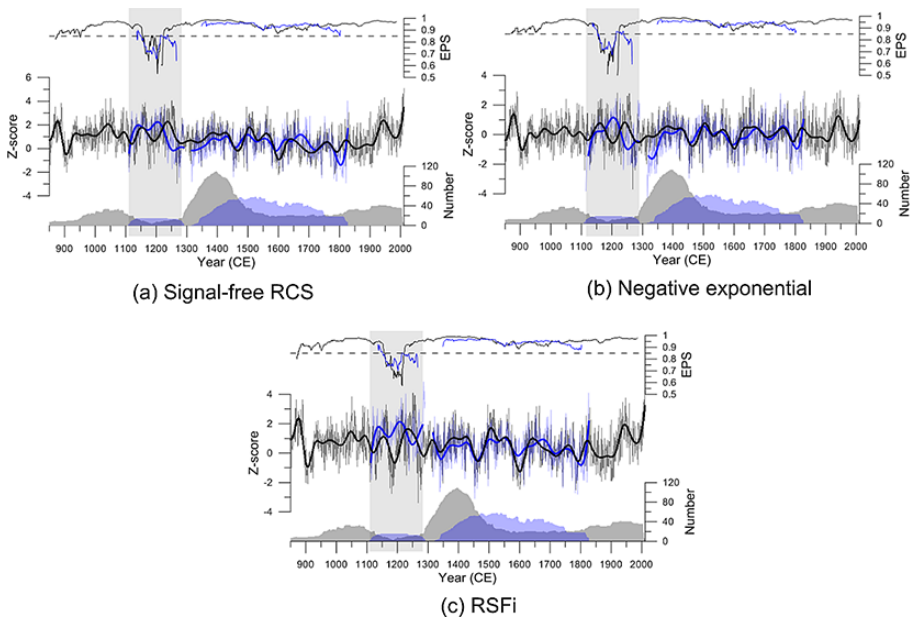

Figure 5. Comparison of the z scored (based on 1700–1800ĊE) interannual (thin curves in the middle subplot) and multidecadal (50 year spline) (bold curves in the middle subplot) variability of the historical (blue) and "in-situ" sample based (black) chronologies after **(a)** signal-free RCS standardisation (smoothed by age-dependent spline), **(b)** negative exponential curve standardisation and **(c)** RSFi standardisation. Sample replication and EPS information was given in the lower and upper subplot. The low EPS time period around 12th century was marked with a shaded background.

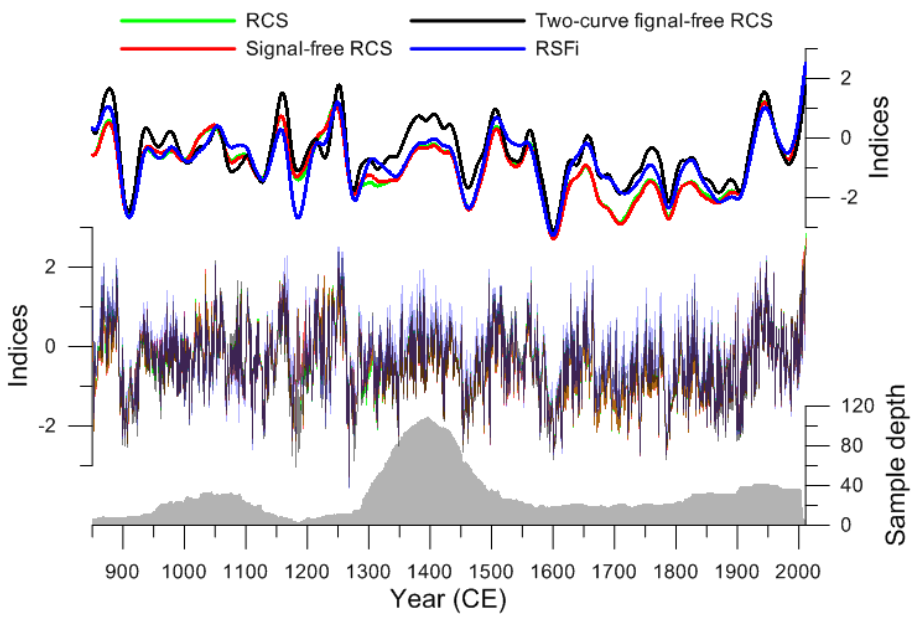

Figure 6. Comparison of the interannual (thin curves in the middle subplot) and multidecadal (50 year spline) (bold curves in the upper subplot) variability in the mean-adjusted 238 field-sample based chronologies based on RCS standardisation (smoothed by hugershoff function) (green curves), one-curve signal-free RCS standardisation (smoothed by age-dependent spline)(red curves),two-curve signal-free RCS standardisation (smoothed by age-dependent spline) (black curves) and RSFi standardisation (blue curves). Sample replication was given in the lower subplot.

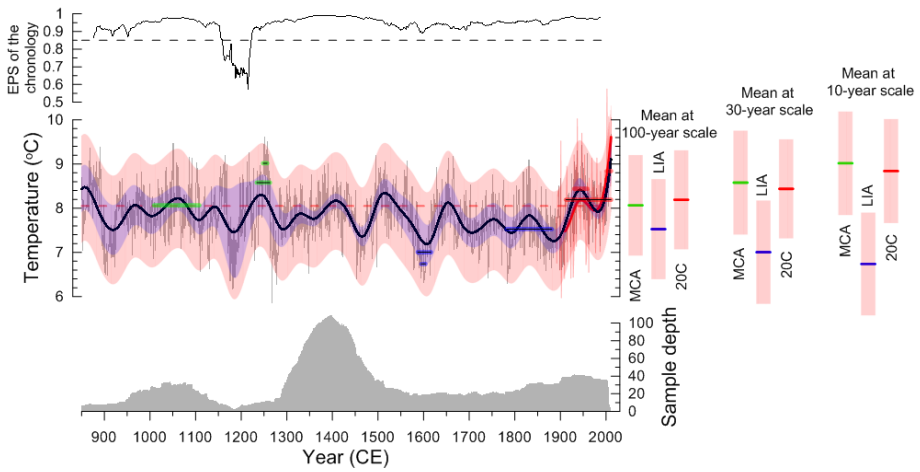

Figure 7. Annual (grey) and 80 year spline filtered (bold black) warm-season temperature variability over the period 850–2011 CE inferred from the new chronology in this study. Purple and pink shading indicate the chronology uncertainty and the total uncertainty of the reconstruction (including chronology uncertainty and reconstruction uncertainty), as expressed as the $2\times$ the standard error in their upper and lower limitations. The grey shading and the thin black curve indicate the sample depth and EPS values (with the dashed line show the threshold of 0.85) of the chronology. Observed annual and 80 year spline filtered warm-season temperature is shown by the thin red curve and the bold curve, with the red dashed line indicating the 1961–1990 mean. The short lines in the right part of the panel mark the mean temperature levels of the warmest 100, 30 and 10 years in MCA (10th–13th century (Grove and Switsur, 1994)) (green) and 20th century (red), and the coldest 100, 30 and 10 years in the LIA (14th–19th century (Grove, 2001)) (blue). The time spans are marked on the corresponding positions on the temperature curve. The coloured short lines with thin solid black line in the centre mark the time spans of the warmest and coldest 100, 30 and 10 years during the past 1200 years.

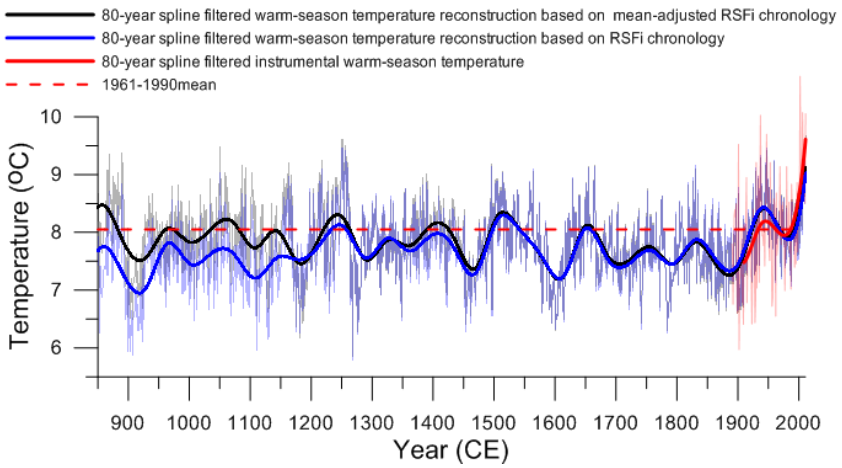

Figure 8. Comparison of the reconstructed warm-season temperature based on the mean-adjusted MXD samples (black) and the unadjusted MXD samples (blue). Red curves show the observed warm-season temperature variability. Light curves indicate the interannual variability, and the bold curves show the variability smoothed by 80 year spline filter. Dashed line shows the observed 1961–1990 mean warm-season temperature.

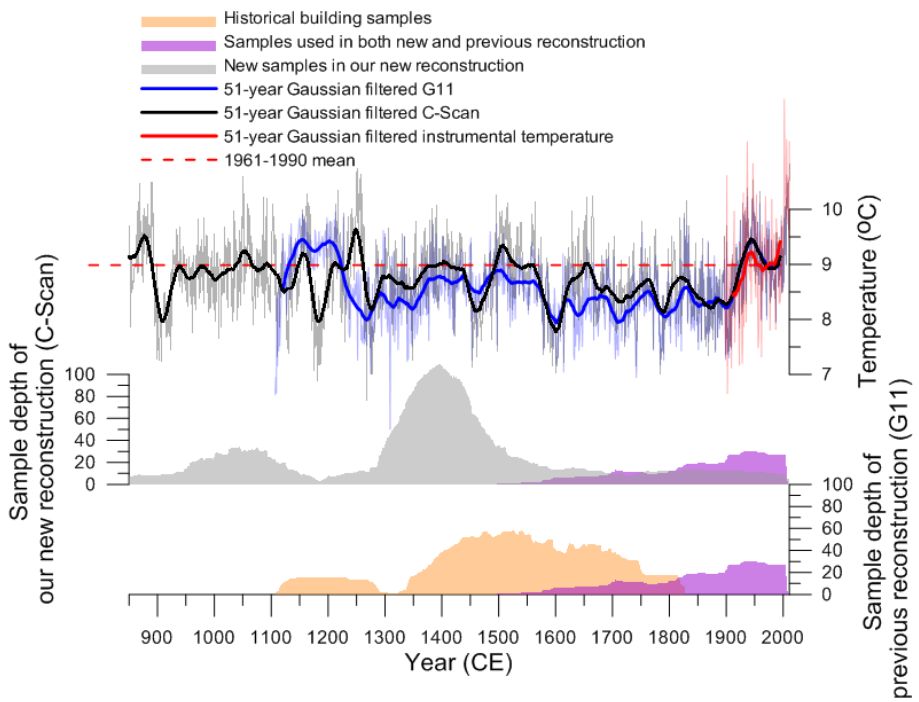

Figure 9. Comparison of C-Scan (thin grey curve) with the previous tree-ring MXD based central Scandinavia warm-season temperature reconstruction (thin blue curve, Gunnarson et al., 2011). Bold black and blue curves show the variability after 51-year Gaussian filtering. The sample depths (number of trees) of the two reconstructions are marked by the black and purple (C-Scan) and orange and purple (G11) shadings. The red curves indicate the observational temperature variability and its 51-year Gaussian filtered variability. The dashed red curve marks the observed 1961-1990 mean temperature.

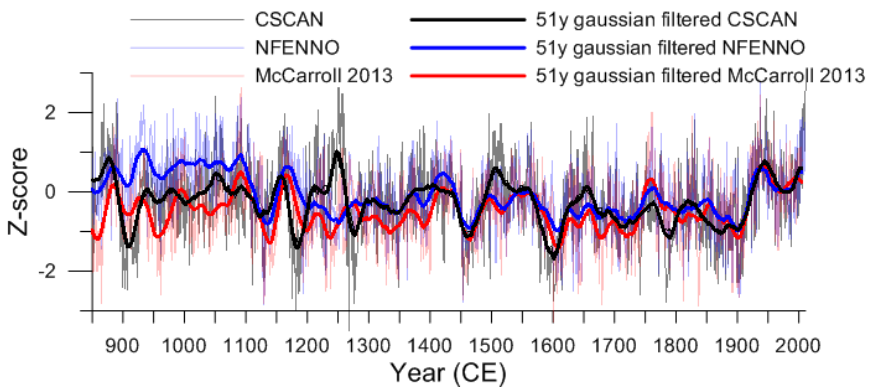

Figure 10. Comparison between C-Scan (black) with tree-ring MXD based northern Fennoscandia (NFENNO) summer temperature reconstruction (blue) (Matskovsky and Helama , 2014) and multi-proxy based northern Fennoscandia summer temperature reconstruction (red) (McCarroll et al., 2013). Bold curves show the variability after 51-year Gaussian filtering. z scores were calculated based on 1890–2005 CE.

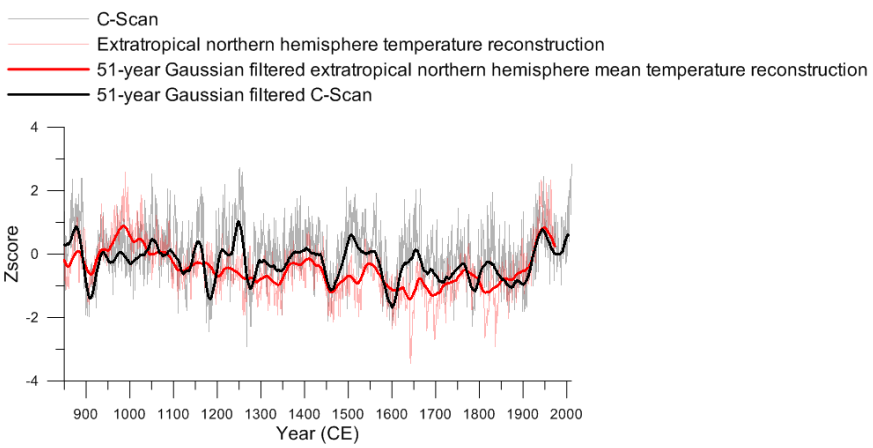

Figure 11. Comparison between C-Scan (thin grey curve) and the extratropical northern hemisphere multi-proxy annual mean temperature reconstruction (thin red curve, Christiansen and Ljungqvist , 2012) during 851–1973 CE. Bold black and red curves show the variability after 51-year Gaussian filtering. z scores were calculated based on 1850–1973 CE.